# Characterization of Surface Breaking Cracks Using One Tangential Component of Magnetic Leakage Field

Reza Khalaj Amineh[1], Natalia K. Nikolova[1], James P. Reilly[1], and James R. Hare[2]

***Abstract*—An inversion procedure is proposed for full characterization of rectangular surface breaking cracks based on measurements of only one tangential component of the magnetic field in the magnetic flux leakage (MFL) technique. The parameters of interest include orientation, length and depth of the cracks. We assume that the length and the depth of the investigated cracks are much larger than the crack width such that the variation of the MFL response with respect to the width is negligible. The proposed procedure employs fast direct methods which provide reliable estimation of the crack parameters in three separate consecutive steps. De-noising and correction techniques are proposed as well. The accuracy of the proposed estimation methods is examined via simulations based on the finite element method (FEM) as well as experimental MFL data.**

***Index Terms*—non-destructive testing, magnetic flux leakage technique, crack sizing, inversion.**

## I. Introduction

The ability to accurately assess the geometry of a defect in a ferromagnetic material is of critical importance for the non-destructive testing (NDT) of oil and gas pipelines using the magnetic flux leakage (MFL) inspection. The MFL technique involves magnetizing the pipe in the axial or the circumferential direction and detecting the corresponding magnetic leakage fields using Hall sensors (Fig. 1). A flawed region in the background metal acts as a region of high magnetic reluctance causing an increased leakage field. Thus, the MFL response due to the defect alone can be obtained by subtracting the background signal from the total measured signal [1]. The ultimate objective of MFL data analysis is to predict the maximum safe operating pressure for the pipe. It is related to the defect's depth [2][3] and also its length-to-width ratio [4][5]. The latter contributes to the local stress concentrations in the neighborhood of the defect. The most critical defects associated with pipelines are crack-like defects (welding cracks, fatigue cracks, stress corrosion cracks, hydrogen-induced cracks, and sulfide corrosion cracks [6]). For these surface breaking cracks, the length $l$ and the depth $d$ are typically much larger than the crack width $w$ such that the variation of the MFL signal with respect to the width is negligible (Fig. 1). It is also assumed that the investigated cracks are straight along their length and the crack walls are perpendicular to the metal surface. Furthermore, small irregularities in the depth (the bottom of the crack) are ignored since they have negligible effect on the MFL response [7]. Therefore, the parameters of interest are the length $l$ and depth $d$ of the crack.

The location of the peaks in the normal $z$-component (Fig. 1) of the magnetic field gives a proper approximation of the length of a crack which is along the direction of the applied field [4][7]-[9]. However, in practice, cracks may have arbitrary orientations ($\theta$ in Fig. 1). More importantly, the $z$-component of the magnetic field is often not available.

Regarding the depth, calibration of the MFL signals in terms of defect depth has been studied both through finite-element modeling [8]-[12] and through analytical methods [7][13]. However, the obtained calibration curves do not take into account the effect of the crack length on the signal strength. Here, we show that neglecting the crack length in constructing the calibration curves may lead to significant errors in depth estimation.

In this paper, we propose a direct methodology to estimate the crack parameters only from the measured $y$-component (Fig. 1) of the magnetic leakage field in accordance with the available experimental set-up. In order to achieve accurate estimation of the length and the depth, the orientation of the crack ($\theta$ in Fig. 1) is estimated first. Unlike the method presented in [14], where all three components of the magnetic field are used to estimate the orientation, our method uses only the $y$-component. Thus, our method implies much simpler measurement apparatus.

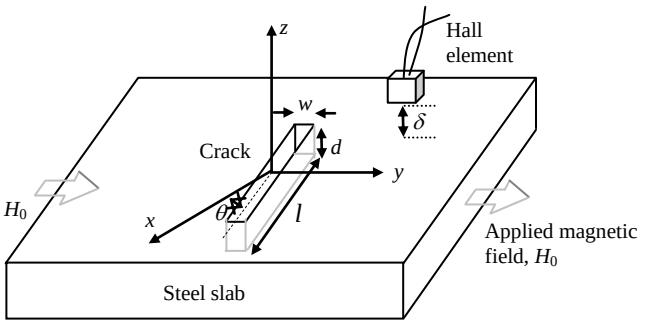


Fig. 1. Illustration of the MFL technique.

[1]Electrical and Computer Engineering Department, McMaster University, Hamilton, ON, Canada L8S4K1.

[2]Intratech Inline Inspection Services Ltd., 3995 Sladeview Cres., Unit 7, Mississauga, ON, Canada L5L 5Y1.

The proposed inversion procedure consists of the following separate direct estimation steps, which must be carried out consecutively: 1) estimation of orientation, 2) estimation of length, and 3) estimation of depth (Fig. 2).

In the first step, the estimation of the orientation is based on the fact that the maximum MFL signal is always along the crack and its direction is across the crack mouth.

In the second step, we use the fact that the locations of the peaks in the first derivative of the MFL response along the crack mouth coincide approximately with the beginning and the ending of the crack. Having these locations, the estimation of the crack length is straightforward. Since this derivative approach is very sensitive to noise especially for near-orthogonal crack orientations where the signal-to-noise ratio is small, we utilize a simple and robust wavelet de-noising algorithm applied to the derivative curves. Wavelet de-noising, especially with soft thresholding [15], has been widely employed with MFL signals [5]-[19] to eliminate high-frequency noise. Here, since we are only interested in the positions of the major peaks in the derivative, we set all the wavelet coefficients corresponding to high-frequency components to zero. This eliminates the ambiguous task of determining proper thresholds.

In the third step, in order to estimate the crack depth, we construct a calibration surface. This surface describes the maximum amplitude of the MFL signal at the crack as a function of the length and the depth of the crack. Once this surface is constructed, the length estimated in the previous step, together with the maximum amplitude of the associated MFL signal, are employed to extract the crack depth. It is worth noting that the calibration surface is constructed for cracks that are parallel to the *x*-axis. For other crack orientations, we propose an appropriate coefficient that adapts the calibration surface.

We examine the accuracy of the proposed method via simulations based on the finite element method (FEM) as well as available experimental MFL data.

## II. Simulation of MFL Response Using FEM

In MFL-type NDT, we deal with a highly nonlinear system involving a permanent magnet and steel. The Maxwell's equations in a nonlinear permanent magnet system lead to [20]:

$$\nabla\times\nabla\times\mathbf{A}=\mu_0(\mathbf{J}+\nabla\times\mathbf{M}) \qquad (1)$$

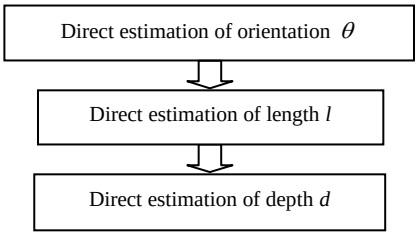


Fig. 2. Inversion procedure for surface breaking cracks using direct methods for estimation of orientation, length, and depth.

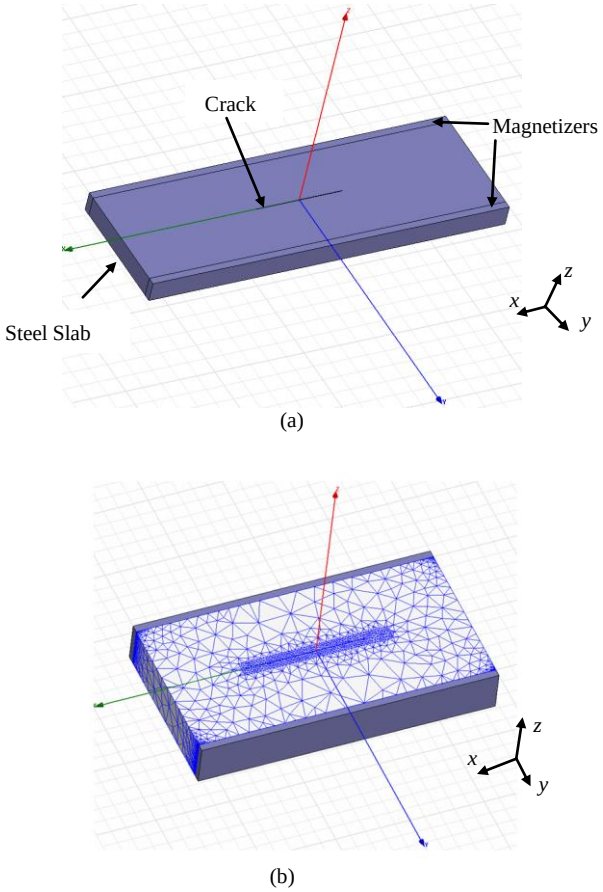


Fig. 3. 3-D view of the simulated model in Maxwell v. 11.1.1: (a) structure, (b) FEM mesh on the surface of the metal slab with enforced refinement of elements in the region around the crack.

where $\mu_0$, **J** and **A** are the magnetic permeability of vacuum, the current density and the magnetic vector potential, respectively. The magnetization **M** is a non-linear function of **H**. Therefore, equation (1) is solved iteratively.

A nonlinear structural FEM using Maxwell v. 11.1.1 [21] is used for simulating three-dimensional (3-D) magnetic field around and inside a surface crack in a steel slab. Fig. 3 shows the model geometry. Steel_1010 is selected from the simulator's library as the material type for the steel slab.

In order to decrease the computational time and still maintain good accuracy, the steel slab is magnetized using two parallel magnets (Fig. 3). NDFe35 is selected as the magnet material. It magnetizes the steel plate in the *y*-direction (Fig. 3) with a coercivity such that the operating point is in the knee area of the B-H curve for Steel_1010. This is desirable because it leads to the maximum signal-to-noise ratio for obtaining the leakage crack signal [20].

We note that the FEM simulations do not match the absolute values of the magnetic field distribution obtained through measurements. However, they match reasonably well with the normalized field distributions.

Some additional boundary conditions are set to enforce the magnetic field inside the metal to be parallel to the *y*-axis. These boundary conditions are: (a) zero normal component of the magnetic field to all faces of the magnetizers except the faces, which are parallel to the *x*-*z* plane; (b) zero tangential

components of the magnetic field at the faces of the magnetizers, which are parallel to the *x*-*z* plane; (c) zero normal component of the magnetic field at the faces of the steel, which are parallel to the *y*-*z* plane.

## III. Direct Method for Estimation of Orientation

We assume that only the $H_y$ field component is available. We integrate $H_y$ along a line $L(\theta)$ which is within the imaged area and is titled at an angle $\theta$ with respect to the *x*-axis as (Fig. 4):

$$f(\theta)=\int_{L(\theta)} H_y dL \tag{2}$$

We refer to $f(\theta)$ as the $\theta$-line integral. We evaluate $f(\theta)$ for all angles $0\le\theta\le180^\circ$ and solve the optimization problem:

$$\theta^*=\arg\max_{\theta} f(\theta). \tag{3}$$

The validity and the accuracy of our technique are tested with data acquired through simulations. This is because all available measurements are associated with nearly $\theta=0^\circ$ orientations. Figures 5(a) to 7(a) show the MFL signal distributions in the *x*-*y* plane monitored at a lift-off distance ($\delta$ in Fig. 1) of 3.5 mm above the metal surface for cracks with *l*=25 mm, *d*=2.2 mm, and actual orientations of $\bar{\theta}=0^\circ$, $60^\circ$, and $85^\circ$. We clearly observe that the maximum of the $H_y$ leakage field component follows the crack. This implies that the $\theta$-line integral attains a maximum value when the line $L(\theta)$ tracks the crack mouth.

Figures 5(b) to 7(b) show the variation of the corresponding $\theta$-line integrals. As predicted, the angle at which the $\theta$-line integral is maximum coincides with the actual orientation of the crack. The accuracy of the orientation estimation is practically independent of the crack length and depth and the results for other cracks are very similar to the ones shown in Figures 5 to 7.

Table I summarizes the results of the estimation of the orientation $\theta^*$ for a range of actual orientations $\bar{\theta}=0^\circ$ to $85^\circ$. We observe that the estimation errors are less than $9^\circ$ when the actual orientation is in the range of $\bar{\theta}=0^\circ$ to $70^\circ$. The estimation suffers larger errors (between $9^\circ$ and $17^\circ$) when the actual orientation is in the range of $\bar{\theta}=70^\circ$ to $80^\circ$. The estimation results are unreliable for actual orientations of more than $80^\circ$. It is clear that the accuracy of the estimated orientation decreases for larger angles $\bar{\theta}$.

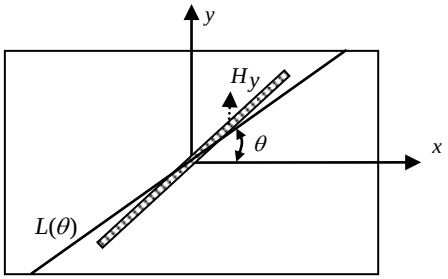


Fig. 4. Schematic of the $\theta$-line integration of $H_y$ along $L(\theta)$.

The reason is that the signal-to-noise ratio (SNR) of the MFL signal is the highest when the crack is perpendicular to the applied field $H_0$ ($\bar{\theta}=0^\circ$) and it decreases as $\bar{\theta}$ tends to $90^\circ$. The relative increase of the noise level with the increase of $\bar{\theta}$ is clearly seen in Figures 5(a), 6(a), and 7(a).

## IV. Direct Method for Estimation of Length

In order to estimate the crack length, we employ the directional derivative of the magnetic field along the crack. We use the estimated orientation of the crack in the previous step to monitor the MFL signal along the crack. The position of the peaks in this derivative gives a proper approximation of the start and end points of the crack.

This method can be applied directly to low-noise signals. However, since the derivative approach could be sensitive to noise in different measurement setups or different crack orientations, we propose a de-noising algorithm based on the wavelet decomposition to discern the desired major peaks in the derivatives from the spurious ones.

### *A. De-noising the Derivatives of MFL Response*

Both simulated and experimental MFL responses may suffer from high-frequency noise such that their derivatives contain a large number of peaks, which are much sharper than the peaks of interest at the two ends of the crack. Therefore, we utilize wavelet de-noising [15]-[19] to reduce these spurious peaks. The derivative of the MFL response monitored along the crack is decomposed at level 3, using a Coiflet wavelet. After setting all the wavelet coefficients corresponding to the details to zero, we reconstruct the signal again. The reconstructed signal does not contain spurious peaks and possesses only a positive and a negative peak at the two ends of the crack.

### *B. Results of the Length Estimation*

Figures 8 to 10 show the MFL responses and their corresponding derivatives for three measured cracks along the *x*-axis ($\bar{\theta}=0^\circ$). These figures also show the same plots obtained from FEM simulations. Here, the MFL signals do not require de-noising because of the high signal-to-noise ratio. The small discontinuities in the derivatives are due to the spatial sampling rate of the measured signal which is 1.5 mm. We have monitored the simulated signals with the same sampling rate.

Table II summarizes the length estimation results for both simulations and measurements for some sample cracks. In both cases, the estimation errors are below 30 percent.

We investigate the robustness of the direct length estimation method for different crack orientations. Figures 11 to 13 show the spatial derivative of the simulated MFL signals along the cracks with *l*=25 mm, *d*=2.2 mm, and actual orientations of $\bar{\theta}=20^\circ$, $60^\circ$, and $80^\circ$. Here, we deal with noisy derivatives and employ the de-noising algorithm. Table III summarizes the results for the length estimation. These results show that length estimation could be achieved with good accuracy for orientations in the range from $0^\circ$ to $75^\circ$.

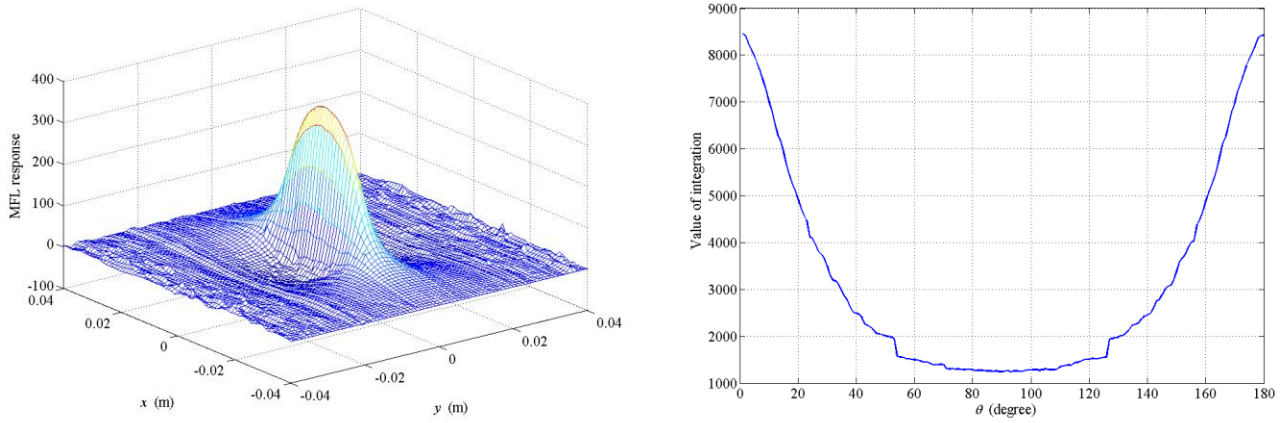


(a) (b)

Fig. 5. (a) Simulated two dimensional distribution of the MFL signal for a crack with *l*=25 mm, *d*=2.2 mm, and $\theta = 0^{\circ}$, (b) the variation of the $\theta$-line integral.

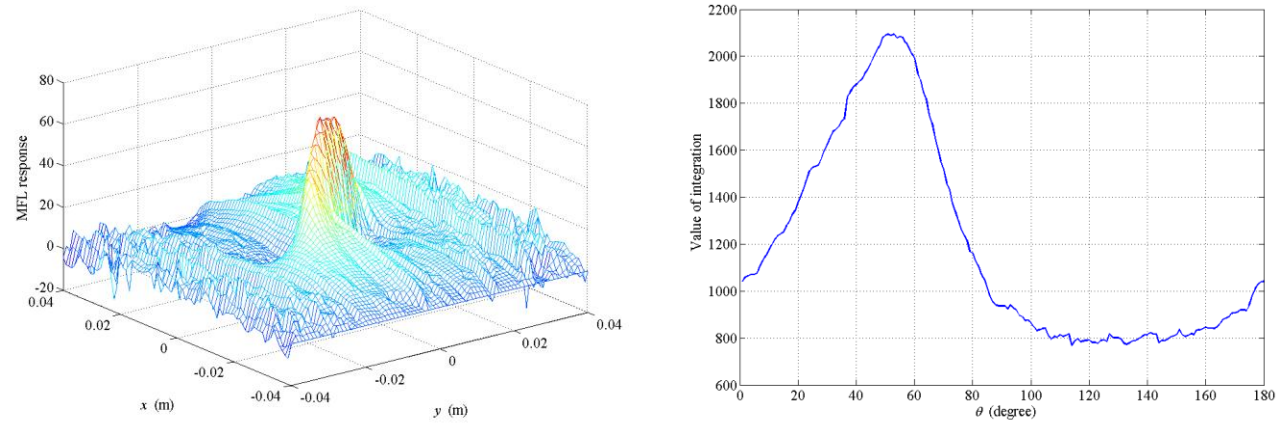


(a) (b)

Fig. 6. (a) Simulated two dimensional distribution of the MFL signal for a crack with *l*=25 mm, *d*=2.2 mm, and $\theta = 60^{\circ}$, (b) the variation of the $\theta$-line integral.

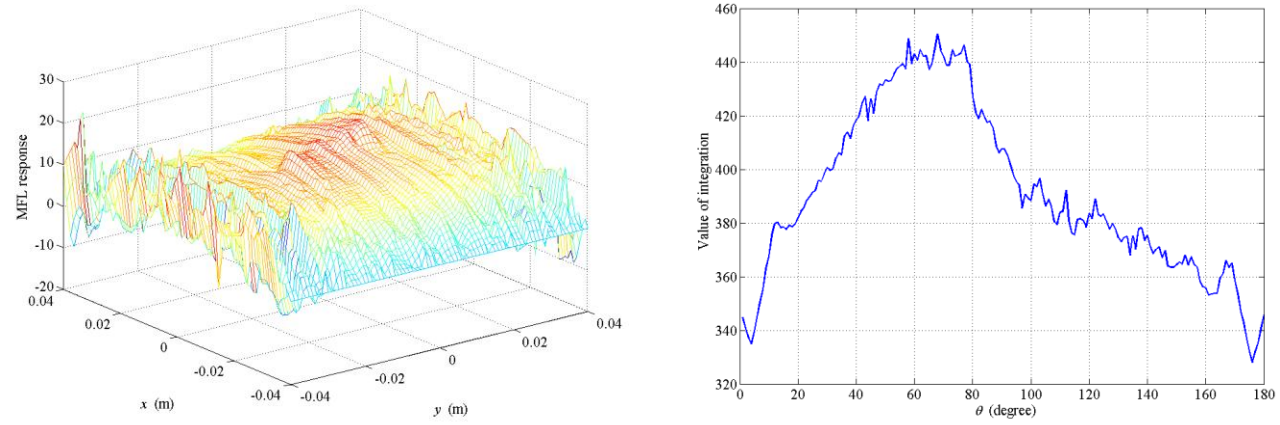


(a) (b)

Fig. 7. (a) Simulated two dimensional distribution of the MFL signal for a crack with *l*=25 mm, *d*=2.2 mm, and $\theta = 85^{\circ}$, (b) the variation of the $\theta$-line integral.

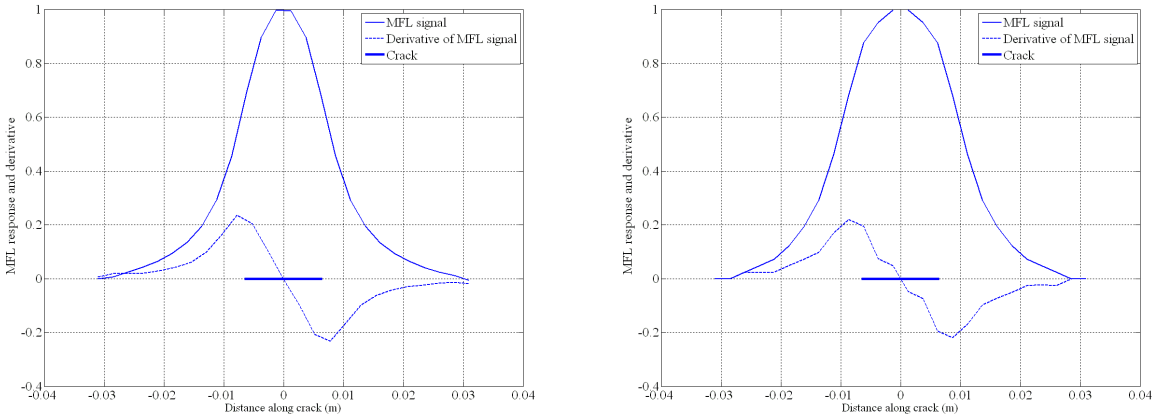


(a) (b)

Fig. 8. Normalized MFL response and its derivative for a crack with $l$=13 mm, $d$=2.2 mm, and $\theta = 0^{\circ}$: (a) simulation, (b) measurement.

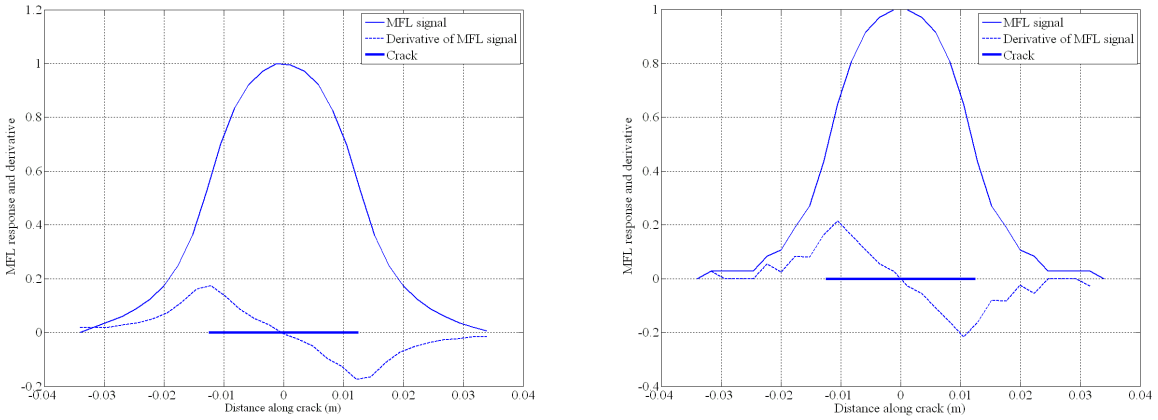


(a) (b)

Fig. 9. Normalized MFL response and its derivative for a crack with $l$=25 mm, $d$=2.2 mm, and $\theta = 0^{\circ}$: (a) simulation, (b) measurement.

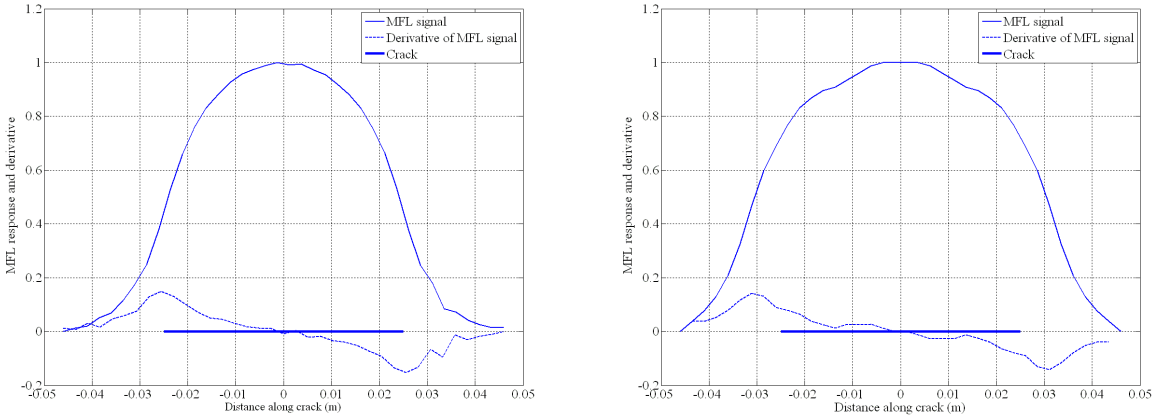


(a) (b)

Fig. 10. Normalized MFL response and its derivative for a crack with $l$=50 mm, $d$=2.2 mm, and $\theta = 0^{\circ}$: (a) simulation, (b) measurement.

TABLE I
ESTIMATION OF ORIENTATION FOR SIMULATED MFL SIGNALS FOR A CRACK WITH L=25 MM AND D=2.2 MM

| Actual angle $\bar{\theta}$ (degree) | Estimated Angle $\theta^*$ (degree) |
|---|---|
| 0 | 0 |
| 20 | 18 |
| 60 | 54 |
| 70 | 61 |
| 75 | 65 |
| 80 | 63 |
| 85 | 68 |

TABLE II
ESTIMATION OF LENGTH USING DERIVATIVE APPROACH

| Crack parameters (mm) | Estimated length $l^*$ (mm) with simulation | Estimated length $l^*$ (mm) with measurement |
|---|---|---|
| $d$=1.2 , $l$=13 | 15.6 | 12.6 |
| $d$=2.2 , $l$=13 | 15.4 | 16 |
| $d$=3.3 , $l$=13 | 15.6 | 10.4 |
| $d$=1.2, $l$=25 | 25.4 | 22 |
| $d$=2.2, $l$=25 | 24.2 | 21 |
| $d$=3.3, $l$=25 | 25.8 | 32 |
| $d$=1.2, $l$=50 | 50.6 | 56 |
| $d$=2.2, $l$=50 | 51 | 62 |
| $d$=3.3, $l$=50 | 50 | 56 |

TABLE III
ESTIMATION OF LENGTH FOR A CRACK WITH L=25 MM, D=2.2 MM, AND DIFFERENT ORIENTATIONS

| Actual angle $\bar{\theta}$ (degree) | Estimated length $l^*$ (mm) |
|---|---|
| 0 | 28 |
| 20 | 28 |
| 60 | 28 |
| 70 | 28 |
| 75 | 28 |
| 80 | --- |
| 85 | --- |

TABLE IV
ESTIMATION OF LENGTH FOR A CRACK WITH L=25 MM AND D=2.2 MM SCANNED AT DIFFERENT LIFT-OFF DISTANCES

| Lift-off distance $\delta$ (mm) | Estimated length $l^*$ (mm) |
|---|---|
| 0.5 | 28 |
| 1 | 28 |
| 2.5 | 28 |
| 4 | 27 |

For orientations above $80^\circ$, the signal-to-noise ratio is not large enough and the desired peaks in the derivative could not be discerned from the spurious ones. We next investigate the effect of the lift-off distance $\delta$ on the accuracy of the proposed length estimation method. Table IV summarizes the results for length estimation with different lift-off distances. The results confirm the robustness of the length estimation method to variations of the lift-off distance.

## V. DIRECT METHOD FOR DEPTH ESTIMATION

In order to estimate the crack depth directly, we use a calibration surface, which describes the maximum of the MFL response with respect to the length and depth of the crack. We construct this surface using measurement results for a sample set of artificially manufactured cracks. In order to evaluate this surface for other cracks with different lengths and depths, we employ appropriate interpolation and extrapolation technique.

Table V shows the length and depth for the 9 measured cracks. It is worth noting that the maximum amplitude of the MFL response is considered after subtracting the background signal [1]. Fig. 14 shows the constructed normalized calibration surface for these 9 measured cracks. We use the following two dimensional inter/extrapolation formula to evaluate the calibration surface *M* at any length and depth:

$$M(l,d) = A \cdot l + B \cdot d + C \cdot l \cdot d + D \qquad (4)$$

where *A*, *B*, *C*, and *D* are constants. The formula in (4) requires four points (cracks) to define a surface element *M*. Since we have 9 cracks with length and depth values of all combinations of $l$ =13, 25, 50 mm and $d$ =1.2, 2.2, 3.3 mm, we define 4 surface elements for inter/extrapolation in different parameter regions, each being described by a set of (*A*, *B*, *C*, *D*) coefficients. Table VI shows the cracks that are used to define the four different surfaces.

Once we have an estimation of the length of the cracks, we can use the maximum of the measured signals and also the calibration surface to obtain an estimation of the depth. Generally, an optimization procedure can be employed for this purpose. However, formula (4) allows for a direct computation of the depth from the estimated length and the maximum of the MFL signal:

$$d^* = \frac{M - A \cdot l^* - D}{B + C \cdot l^*} \qquad (5)$$

where $M$ is the maximum of the signal; *A*, *B*, *C*, and *D* are the computed constants for the element in the parameter region, and $l^*$ is the estimated crack length.

### A. Results for the Depth Estimation

Table VII summarizes the results for the depth estimation of the same 9 measured cracks which were used to construct the calibration surface. Column 2 shows the results when the calibration surface employs all 9 cracks and thus consists of 4 surface elements. We observe that there are errors in the depth estimation despite the fact that the estimated cracks coincide

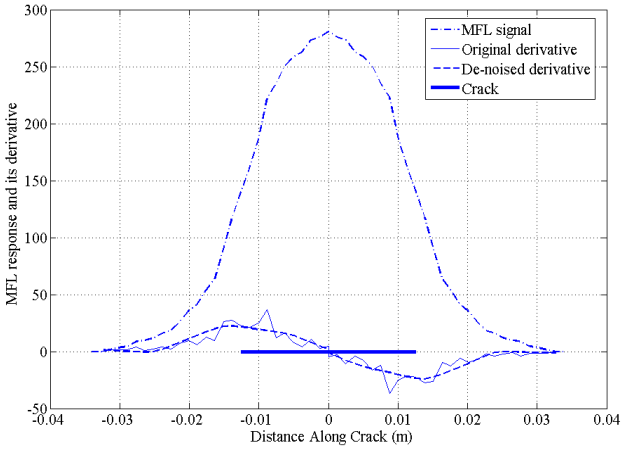


Fig. 11. Derivative of the simulated MFL signals for a crack with $l$= 25 mm, $d$=2.2 mm, and $\theta = 20^{\circ}$.

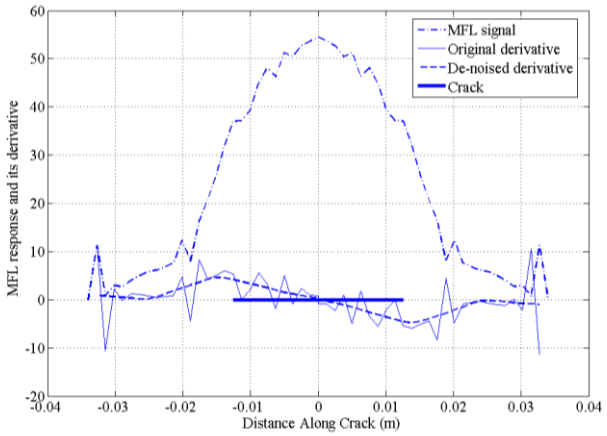


Fig. 12. Derivative of the simulated MFL signals for a crack with $l$= 25 mm, $d$=2.2 mm, and $\theta = 60^{\circ}$.

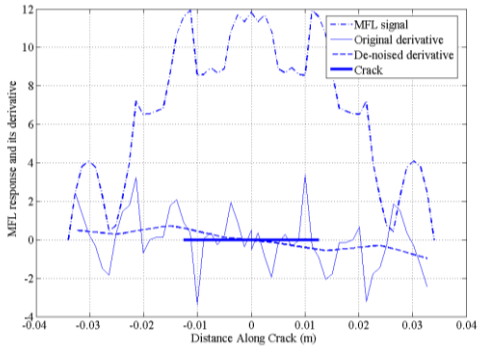


Fig. 13. Derivative of the simulated MFL signals for a crack with $l$= 25 mm, $d$=2.2 mm, and $\theta = 80^{\circ}$.

with the nodes of the calibration surface. This is because the calibration surface is constructed using the known (true) length $\bar{l}$ and depth $\bar{d}$ of the cracks while the estimated depth $d^*$ is obtained from the estimated length $l^*$ where, generally, $l^* \neq \bar{l}$.

The highest inversion errors occur in the case of ignoring calibration for $d$=1.2 mm. This corresponds to extrapolation from known cracks with depths of 2.2 mm and 3.3 mm toward smaller crack depths for which we assume the data are not available. In this case, the highest estimation error is 70% for the crack with $l$=13 mm and $d$=1.2 mm. On the other hand, when we ignore calibration for larger depths, the estimation errors are still lower than 28%. Thus, our depth estimations are fairly accurate when extrapolating the calibration surface for deeper cracks. When we ignore calibration points of intermediate depths ($d$=2.2), the inversion errors are lower than 19%.

### *B. Correction of Calibration Surface for Different Crack Orientations*

The calibration surface in Fig. 14 is provided for the case where the orientation of the crack is perpendicular to the external applied field ($\theta = 0^{\circ}$). However, when the crack has any other orientation, the amplitude of the MFL signal weakens and the provided calibration surface needs to be corrected. We propose a simple technique similar to [22] to take into account this change in amplitude. As Fig. 15 shows, when the crack has a non-zero orientation, we could find the projection of the applied magnetic field $H_0$ on an axis perpendicular to the crack ($y'$ in Fig. 15) as:

$$H_0' = H_0 \cos\theta. \qquad (6)$$

Therefore, we can predict that the maximum amplitude of the crack signal changes with the same coefficient $\cos\theta$. Thus, the calibration surface constructed for cracks with $\theta = 0^{\circ}$ is corrected using the factor $\cos\theta$.

TABLE V
PARAMETERS OF THE MEASURED CRACKS

| Crack No. | Length, $l$ (mm) | Depth, $d$ (mm) |
|---|---|---|
| Crack 1 | 13 | 1.2 |
| Crack 2 | 13 | 2.2 |
| Crack 3 | 13 | 3.3 |
| Crack 4 | 25 | 1.2 |
| Crack 5 | 25 | 2.2 |
| Crack 6 | 25 | 3.3 |
| Crack 7 | 50 | 1.2 |
| Crack 8 | 50 | 2.2 |
| Crack 9 | 50 | 3.3 |

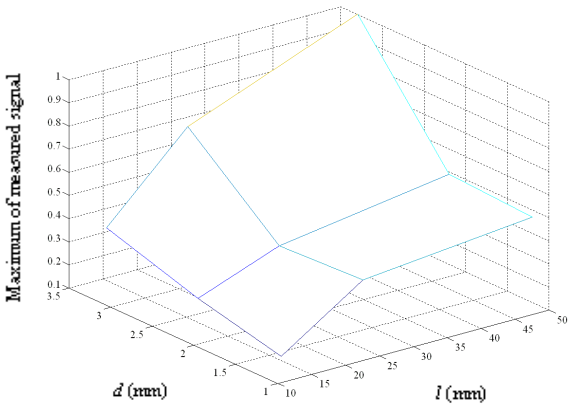


Fig. 14. Normalized calibration surface for the measured cracks.

TABLE VI

MEASURED CRACKS USED TO CONSTRUCT THE CALIBRATION SURFACE IN THE DESIRED REGIONS

| Crack No. in Table V | Parameter Region |
|---|---|
| 1, 2, 4, 5 | $l \le 25$ mm , $d \le 2.2$ mm |
| 2, 3, 5, 6 | $l \le 25$ mm , $d \ge 2.2$ mm |
| 5, 6, 8, 9 | $l \ge 25$ mm , $d \ge 2.2$ mm |
| 4, 5, 7, 8 | $l \ge 25$ mm , $d \le 2.2$ mm |

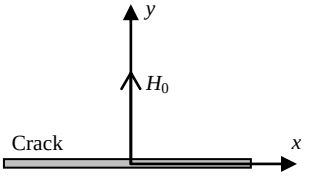


(a)

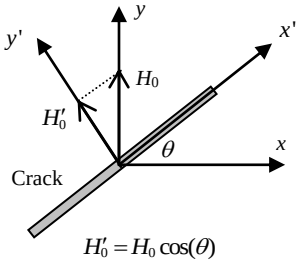


(b)

Fig. 15. (a) Crack with orientation of zero ( $\theta = 0^\circ$ ); (b) illustration of finding the correction factor for a crack with non-zero orientation ( $\theta \neq 0^\circ$ ).

## VI. CONCLUSION

We have developed and validated an inversion procedure to estimate surface breaking crack parameters, i.e., orientation, length, and depth, from single-component magnetic field measurements. The procedure consists of the following consecutive steps: estimation of orientation, estimation of length, and estimation of depth. The direct methods for estimation of orientation and length are fast and robust with respect to various lift-off distances. However, these estimations become increasingly unreliable when the crack is oriented along the magnetizing field. The results for the direct depth estimation demonstrate that when the calibration surface employs cracks, whose parameters span all possible values, we can obtain accurate estimates. We observe that extrapolation toward larger crack depths is reliable as it yields estimate errors below 28%.

## REFERENCES

[1] S. O'Connor, L. Clapham, and P. Wild, "Magnetic flux leakage inspection of tailor-welded blanks," *Meas. Sci. Technol.*, vol. 13, no. 2, pp. 157-162, Feb. 2002.

[2] A. Joshi1, L. Udpa, S. Udpa, and A. Tamburrino, "Adaptive wavelets for characterizing magnetic flux leakage signals from pipeline inspection," *IEEE Trans Magn.*, vol. 42, no. 10, pp. 3168- 3170, Oct. 2006.

[3] F. M. Haggag, "Innovative SSM technology determines structural integrity of metallic structures: example applications for pressure vessels and oil and gas pipelines," *Int. J. Pure and Appl. Phys.*, vol. 3, no. 1, pp. 91-108, Mar. 2007.

[4] C. Mandache and L. Clapham, "A model for magnetic flux leakage signal predictions," *J. Phys. D: Appl. Phys.*, vol. 36, no. 20, pp. 2427-2431, Oct. 2003.

TABLE VII
DEPTH ESTIMATION WHEN CALIBRATING WITH ALL CRACKS AND WHEN IGNORING CALIBRATION FOR SOME DEPTHS

| Crack parameters (mm) | Calibration with all cracks | | Ignoring calibration for $d$=1.2 mm | | Ignoring calibration for $d$=2.2 mm | | Ignoring calibration for $d$=3.3 mm | |
|---|---|---|---|---|---|---|---|---|
| | $d^*$ (mm) | Error (%) | $d^*$ (mm) | Error (%) | $d^*$ (mm) | Error (%) | $d^*$ (mm) | Error (%) |
| $d$=1.2 , $l$=13 | 1.21 | 0.8 | 0.35 | 70 | 1.21 | 0.8 | 1.21 | 0.8 |
| $d$ =2.2 , $l$=13 | 2.28 | 3 | 2.28 | 3.6 | 2.6 | 18.18 | 2.24 | 1.8 |
| $d$ =3.3 , $l$=13 | 3.31 | 0.3 | 3.31 | 0.3 | 3.3 | 0 | 2.5 | 24 |
| $d$ =1.2 , $l$=25 | 1.3 | 8 | 1.25 | 4.1 | 1.38 | 15 | 1.37 | 14.16 |
| $d$ =2.2 , $l$=25 | 2.11 | 4 | 2.09 | 5 | 2.22 | 0.9 | 2.11 | 4 |
| $d$ =3.3 , $l$=25 | 2.42 | 26 | 2.42 | 26.6 | 2.8 | 15 | 2.39 | 27.57 |
| $d$ =1.2 , $l$=50 | 1.15 | 4.1 | 0.48 | 60 | 1.13 | 5.8 | 1.15 | 4.1 |
| $d$ =2.2 , $l$=50 | 1.85 | 15 | 1.61 | 26.81 | 2.03 | 7.72 | 1.85 | 15.9 |
| $d$ =3.3 , $l$=50 | 2.86 | 13 | 2.86 | 13.33 | 2.96 | 10.3 | 2.6 | 21.21 |

[5] R. C. Juvinall, *Engineering Considerations of Stress, Strain, and Strength*, New York: McGraw-Hill, 1967, chapter 13.
[6] L. W. Tsay, Y. C. Chen, S. L. I. Chan, "Sulfide stress corrosion cracking and fatigue crack growth of welded TMCP API 5L X65 pipeline steel," *Int. J. Fatigue*, vol. 23, no. 2, pp. 103-113, Jan. 2001.
[7] C. Edwards, S. B. Palmer, "The magnetic leakage field of surface-breaking cracks," *J. Phys. D: Appl. Phys.*, vol. 19, no. 4, pp 657-673, Apr. 1986.
[8] W. Lord and J. H. Hwang, "Defect characterization from magnetic flux leakage fields," *British J. NDT*, vol. 19, no. 1, pp. 14-18, Jan. 1977.
[9] E. Altschuler and A. Pignotti, "Nonlinear model of flaw detection in steel pipes by magnetic flux leakage," *NDT&E Int.*, vol. 28, no. 1, pp. 35-40, Feb. 1995.
[10] D. L. Atherton and M.G. Daly, "Finite Element Calculation of Magnetic Flux Leakage Detector Signals," *NDT&E Int.*, vol. 20, no. 4, pp. 235-238, Aug. 1987.
[11] W. Lord, J. M. Bridges, W. Yen, and R. Palanisamy, "Residual and active leakage fields around defects in ferromagnetic materials," *Mat. Eval.*, vol. 36, pp. 47-54, Jul. 1978.
[12] S. Mandayam, L. Udpa, S. S. Udpa, and W. Lord, "Invariance transformations for magnetic flux leakage signals," *IEEE Trans. Magn.*, vol. 32, no. 3, pp. 1577-1580, May 1996.
[13] J. Philip, C. B. Rao, T. Jayakumar, B. Raj, "A new optical technique for detection of defects in ferromagnetic materials and components," *NDT&E Int.*, vol. 33, no. 5, pp. 289-295, Jul. 2000.
[14] Y. Li, J. Wilson, and G. Y. Tian, "Experiment and simulation study of 3D magnetic field sensing for magnetic flux leakage defect characterization," *NDT& Int.*, vol. 40, no. 2, pp. 179-184, Mar. 2007.
[15] D. L. Donoho, "De-noising by soft-thresholding," *IEEE Trans Inf. Theory*, vol. 41, no. 3, pp. 613-627, May 1995.
[16] M. Afzal, S. Udpa, "Advanced signal processing of magnetic flux leakage data obtained from seamless gas pipeline," *NDT&E Int.*, vol. 35, no. 7, pp. 449-457(9), Oct. 2002.
[17] M. Afzal, R. Polikar, L. Udpa, and S. Udpa, "Adaptive noise cancellation schemes for magnetic flux leakage signals obtained from gas pipeline inspection," *IEEE Int. Conf. on Acoustics, Speech, and Signal Processing (ICASSP '01)*, vol. 6, pp. 3389-3392, May 2001.
[18] W. Han, P. Que, "A modified wavelet transform domain adaptive FIR filtering algorithm for removing the SPN in the MFL data," *Meas.*, vol. 39, no. 7, pp. 621-627, Aug. 2006.
[19] J. Tao, Q. Peiwen, C. Liang, and L. Liang, "Research on a recognition algorithm for offshore-pipeline defects during magnetic-flux inspection," *Defektoskopiya*, vol. 41, no. 4, pp. 34-43, Apr. 2005.
[20] G. S. Park, E. S. Park, "Improvement of the sensor system in magnetic flux leakage-type nondestructive testing (NDT)," *IEEE Trans. Magn.*, vol. 38, no. 2, pp. 1277-1280, Mar. 2002.
[21] Maxwell Version 11.1.1, Ansoft Corporatin, http://www.ansoft.com, 2006.
[22] Y. Melikhov, S. J. Lee, D. C. Jiles, R. Lopez, and L. Brasche, "Analytical approach for fast computation of magnetic flux leakage due to surface defects," *Digests of the IEEE Int. Magnetics Conference (INTERMAG)*, Apr. 2005.